

# A Compilation Framework for Photonic One-Way Quantum Computation

Hezi Zhang<sup>1</sup>, Anbang Wu<sup>1</sup>, Yuke Wang<sup>1</sup>, Gushu Li<sup>1</sup>, Hassan Shapourian<sup>2</sup>, Alireza Shabani<sup>2</sup> and Yufei Ding<sup>1</sup>

<sup>1</sup>University of California, Santa Barbara

<sup>2</sup>Cisco Systems, Inc.

**Abstract**—Compared to solid-state quantum qubits (e.g., superconducting transmons), flying photonic qubits have several advantages for long-term, large-scale quantum computing. First, quantum computers made from photonic qubits can, in principle, operate at room temperature. They are also one of the best techniques that have the potential to scale up to millions of qubits over a practical timescale. In addition, they can be easily integrated into existing fiber-optic-based telecommunications systems, facilitating the connection of individual quantum computers toward large-scale distributed quantum computing systems.

In this paper, we propose the first end-to-end compilation framework to accommodate one-way quantum computation toward realistic photonic quantum devices. Unlike previous compilation efforts targeting solid-state-qubit quantum technologies, our compilation framework need to deal with a new set of unique features of photonics quantum computing at both programming and hardware levels. For example, all computations are natively conducted in the form of measurements instead of 1-qubit and 2-qubit gates and qubits will be destroyed instantly after the measurements. Being the first work in this direction, we unveil the huge optimization space for mapping a quantum program to photonic devices where computation resources can be saved by orders of magnitude with novel compiler optimization designs.

## I. INTRODUCTION

Quantum computing (QC) is promising in its potential of providing significant speedup to many problems, such as large-number factorization (exponential speedup) [32] and unordered database search (quadratic speedup) [16]. On the hardware side, a list of computing technologies has achieved promising progresses toward physical realization in both research lab settings and industrial production levels, including superconducting [13], ion trap [11], neutral atoms [31], and photonics [19]. There is not yet a clear winner and it is anticipated that multiple technologies will develop together and serve different mission needs and application requirements.

Recently, there is a surge of interest on photonic quantum computing [28], [34]. This is not only because of the unique features of photonic devices [6], [27] (e.g., great scalability, easy integration with network), but also due to breakthroughs in photonic technologies [22], [26], [36] and the successful demonstration of quantum supremacy on photonics-based quantum computers [24], [37], [38]. PsiQuantum [3], [5], [7] also recently announces the world’s first manufacturing milestone in photonic quantum computing, with quantum photonic and electronic chips being manufactured using the advanced semiconductor tools.

Yet, photonic quantum computing also presents a new set

of challenges that cannot be directly handled by conventional programming and compiler frameworks [1], [33] targeting the quantum circuit model [25]. First, in photonic systems, single-qubit measurements in arbitrary bases can be implemented on a single universal chip [20] by combining reconfigurable single-qubit gates and photon detectors, but not general 2-qubit gates as opposed to those in other quantum computing systems [11], [13], [31]. Second, measurements on photons are destructive [20], which means that photons will vanish once they are measured and thus the information stored in those qubits shall be safely transferred to some other qubits along with the measurement results and new qubits need to be generated to replace them for future computations. Third, a special type of two-qubit entangling measurements, called fusions [10], [20], can be performed to create entanglements among two groups of qubits, but at the cost of destroying two qubits directly involved in the measurements

Fortunately, at programming level, measurement-based quantum computing (MBQC) [29], another universal programming paradigm in contrast to the widely used circuit model [25], can be regarded as a native programming paradigm for programming general quantum applications on photonics devices. In this programming paradigm, an arbitrarily large, entangled resource state (e.g., the so-called cluster state [29], [30]) is assumed to be prepared prior to the computation using a fixed pattern of devices that generates uniform entanglement among qubits and then various tasks can be performed by a series of single-qubit projective measurements on the resource state. During the computation, each qubit is measured only once and is then free to detach from the computing system or even disappear. This is why MBQC is also called “one-way” quantum computing model.

But few attempts have been done on the compilation side. Previous work [8], [29], [35] primarily focuses on proving that the MBQC is theoretically equivalent to the circuit model by turning operations in a quantum circuit into native operations in the MBQC paradigm, which can serve as a basic transpilation flow from quantum circuits to MBQC. Existing approaches in MBQC can be categorized into two types. The first type assumes a large enough cluster state [29], [30] in a regular lattice coupling structure. Qubits and gates in a quantum circuit can be directly mapped to operations on the cluster state, with this cluster state realized by some underlying MBQC machines [15]. However, the regular cluster

state itself in this compilation flow brings significant overhead by introducing redundant qubits and measurement operations. Moreover, on a realistic photonics quantum computer, the hardware can only generate small resource states. Cascading them into large states also introduces significant overhead due to the expensive state merging operations (e.g., fusion operations [10]). The second type of approaches [9] starts from converting the input quantum program into a graph state whose edges directly indicate the necessary entanglements for the targeted program. Thus it leads to a relatively small overhead but high irregular structure. It is not yet known how we can efficiently map an irregular graph state onto an MBQC machine with hardware-constrained capability of generating small resource states.

In this paper, we investigate how to optimize the quantum program compilation onto a photonics-based MBQC machine. As the first step, we formulate the hardware model of a photonics-based quantum computer and identify the key challenges in compilation on such an MBQC architecture. We abstract the hardware model to a *flattened temporal-spatial hierarchy coupling graph* by flattening the original 3D coupling structure into a concatenation of 2D layers of physical qubits. This on one hand naturally represents hardware resources (e.g., resource state generators) and constraints (e.g., available photon routing through fibers), and on the other hand captures the planar-extensibility of the hardware that can be leveraged to benefit the follow-up compilation design. Upon such a hardware abstraction, we identify three key compilation challenges: 1) lack of native high-degree node support on hardware, 2) mismatch between the irregular structure of program entanglement and the regular structure of physical couplings supporting fusion operations, and 3) limited generation speed and lifetime of physical resource states. In the meantime, we observe that the *non-planarity* in geometry of graph states representing the input programs is the key to these challenges as it prevents efficient qubit/operation mapping and creates conflicts in operation scheduling.

To this end, we propose an end-to-end compilation framework to tackle all these challenges with three key modules. The first module is the **Fusion Graph Generation** (Section IV). This module synthesizes the graph state representation of a quantum program containing arbitrarily high-degree qubit nodes from low-degree nodes in resource states through proper fusion strategies. After resolving the high-degree node issue, the second module, **2D-Lattice Mapping and Routing** (Section V), finds a compatible embedding to deploy the input program onto the hardware architecture with 2D lattice fusion operation support. By winding the edges along the flattened temporal-spatial hierarchy coupling graph and penalizing long paths, we can minimize the overhead of extra fusions and prevent long qubit endurance time requirement. The third **Graph Partition and Scheduling** module (Section VI) partitions the graph of an input program and schedules it onto individual or successive layers of qubits in the flattened temporal-spatial hierarchy coupling graph considering both the operation dependency and the graph topology. Note that all the module

designs follow the **Non-Planar Graph Prohibition** philosophy. Non-planar graphs of input programs are decomposed into planar graphs and the planarity is preserved in all modules throughout our compilation flow. With these modules, our framework maximizes the operation throughput and resource utilization to efficiently accommodate the adaptivity of input programs.

Our contributions in this paper are summarized as follows:

- We abstract the hardware model of photonic MBQC to a flattened temporal-spatial hierarchy coupling graph, and propose an end-to-end compilation framework to deploy and optimize quantum program executions on it.
- We identify three critical compilation challenges in the gap between a quantum program and a photonics-based MBQC architecture, and propose corresponding optimization modules to tackle them automatically.
- We make an observation that the non-planarity in the graph representation of input programs is a bottleneck for program mapping and scheduling, and use it as the key to guide the design of the entire compilation flow.
- Our framework outperforms a baseline that relies on static large cluster states by orders of magnitude in execution time and resource consumption of the compiled program.

## II. BACKGROUND AND RELATED WORK

We start with the necessary background about measurement-base quantum computing (MBQC) paradigm. The basic quantum computing concepts (e.g., qubit, gate, linear operator, circuit) are not covered and we recommend [25] for more details.

### A. Programming Paradigm and Compilation in MBQC

Previous works have proved that MBQC is a universal computing paradigm by studying how to theoretically convert a quantum circuit in the circuit model to operations in the MBQC paradigm [29]. These works can be considered as basic and preliminary compilation to execute a quantum circuit on an MBQC machine. They can be categorized into two types and are briefly introduced here.

#### 1) Mapping onto Regular Lattice First

The ‘Mapping onto Regular Lattice First’ approach could translate a circuit in Fig. 1 (a) to a pattern of single-qubit measurement as shown in Fig. 1 (b), with the measurement basis marked on the corresponding qubits. The general computational resource in MBQC is the so-called cluster state [29], which consists of an array of qubits initialized and entangled together with some specific structure. This ‘Mapping onto Regular Lattice’ will first assume that the qubits in the cluster state is coupled in a special regular structure, a 3D lattice [29]. With the qubits in a 3D cluster state, there would be a direct mapping from the logical qubits and gates in a quantum circuit to the operations on the cluster state. We next give some details about the mapping of single-qubit and two-qubit gates.

**Single-Qubit Gate** An arbitrary single-qubit gate can be implemented with single-qubit measurements along different measurement basis on at most four qubits in the logical qubit braid. For example, the Hadamard gate and the  $R(\xi, \eta, \zeta)$  gate

can be implemented by a pattern of measurements in the red circles, while an identity gate can be implemented by inserting two adjacent X-measurements, which can be used to align the patterns of different gates.

Note that for Clifford gates like the Hadamard gate (Fig. 1(a)), the measurement sequence does not have a dependency on the measurement outcomes of any other qubit. That is, all X-, Y-basis measurements can be done simultaneously even if their corresponding gates are at the end of the circuit. But for non-Clifford single-qubit gates, the measurement basis on one qubit may depend on the measurement outcomes of previous qubits. For example, in the measurement pattern of  $R(\xi, \eta, \zeta)$ , the angles of measurement basis in the red circle may need to be adjusted according previous measurement outcomes (e.g., from  $\xi$  to  $\pm\xi$ ).

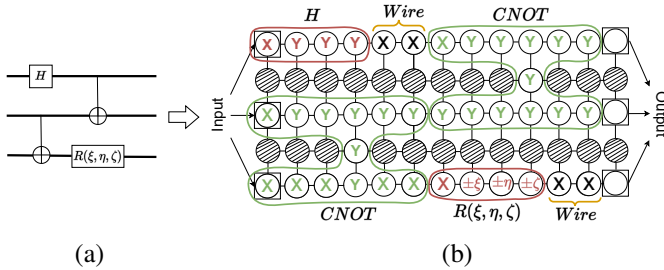


Fig. 1: From a circuit (a) to its MBQC measurement pattern (b), with the measurement bases labeled on the qubits (e.g., X means measuring in X-basis). Patterns in red correspond to the single qubit gates, patterns in green correspond to the CNOT gates. Two adjacent X-measurement can play the role of a wire to align up the patterns, as marked in yellow. Shaded qubits are the ones removed by measurements in Z-basis.

**Two-Qubit Gate** Two-qubit gates applied on two logical qubits are also implemented by single-qubit measurement sequences, with a key difference that there will be measurement patterns to connect those two logical qubits. For example, in Figure 1, the CNOT gates are implemented by the measurement patterns in the green circles on the right and the measurements need to connect the two braids corresponding to the two logical qubits. Similar to the circuit model, CNOT gates on non-neighboring qubits in MBQC can be implemented by inserting measurement patterns of SWAP gates whenever necessary. Redundant qubits (shaded qubits in Figure 1) can be removed by being measured in Z-basis. For more details about the specific measurement patterns for different gates, please refer to [29].

**Drawbacks** The approach simplifies the mapping from qubits and gates in a circuit to measurement operations on a cluster state while it comes with great overhead when deploying the regular 3D cluster state onto a realistic MBQC device. Many qubits are initialized in the cluster state and then disregarded by Z measurement immediately (shaded qubits in Figure 1(b)). The two-qubit gates can be implemented on two adjacently logical qubit braids easily but are much more expensive when applied on logical qubit braids that are not adjacent. Moreover, on a realistic MBQC device like a

photonic quantum computer introduced later in this section, the hardware only generates small sparse cluster states.

## 2) Converting to Graph State First

Instead of embedding the gates into the grid of cluster state, the second approach is to convert the input circuit into a graph state [9] which also can show the measurement sequence required to execute the input circuit in MBQC but do not demand the 3D lattice structure in the cluster state. To turn a circuit into its corresponding graph state, it is first compiled to a universal gate set  $\{J(\theta), CZ\}$  [9], where  $J$  gate is defined as

$$J(\alpha) = \begin{bmatrix} 1 & e^{i\alpha} \\ 1 & e^{-i\alpha} \end{bmatrix} \quad (1)$$

Note that an arbitrary single-qubit gate  $U$  can be decomposed into  $U = e^{i\theta} J(\alpha) J(\beta) J(\gamma)$ .

Figure 2 shows an example of this approach. On the left is the input circuit and its generated graph state is on the right. The node  $a$  corresponds to the qubit A. It connects to three nodes as there are three CZ gates connecting the qubit A to qubit B, C, and D.  $CZ$  is a Clifford gate so there is no dependency regarding the measurements on node  $a$  and node  $b_2, c_2$ , and  $c_2$ . There are also single-qubit  $J$  gates on qubits and they are represented by nodes  $b_1, b_2, b_3$ . There will be a measurement order requirement when the  $J(\theta)$  gate is non-Clifford and we use directed edges to represent such dependency. For example, the edge  $b_1 \rightarrow b_2$  indicates that the measurement basis of  $b_2$  may need to be adjusted according to the measurement outcome of  $b_1$ . We remark that the generated graph state only contains the necessary coupling structure that is purely derived from the input circuit, so that the qubits and coupling requirements are much smaller compared with the first ‘Mapping onto Regular Lattice First’.

**Drawbacks** Unfortunately, it is not yet known how we can efficiently map the graph state onto an MBQC machine, which usually generate small cluster states on physical qubits with a set of other hardware constraints. There is neither any prior work discussing possible graph transformations that could potentially enabling us to resolve the mismatch between the topology of arbitrary graph states with the fixed topology of the underlying hardware. To this end, our work gives an in-depth analysis of the challenges here and build up the first modular compiler to automate the mapping.

## B. MBQC on Photonics Quantum Hardware

We will introduce some basics about the linear optical quantum computing and the key architectural constraints that need to be considered in the compilation optimization. For more details about linear photonics, we recommend [20].

**Photonic qubits** In linear optical quantum computing, a qubit is usually implemented by representing the two basis states  $|0\rangle_L$  and  $|1\rangle_L$  with two optical modes of a fixed photon number. The optical modes can be either two spatial modes ( $|0\rangle_L = |1\rangle \otimes |0\rangle$  and  $|1\rangle_L = |0\rangle \otimes |1\rangle$ , where  $|0\rangle$  and  $|1\rangle$  are the two basis states in one optical mode), referred as ‘dual-rail qubits’, or two polarization modes of a single qubit ( $|0\rangle_L = |H\rangle$  and  $|1\rangle_L = |V\rangle$ , where  $|H\rangle$  and  $|V\rangle$  represent the

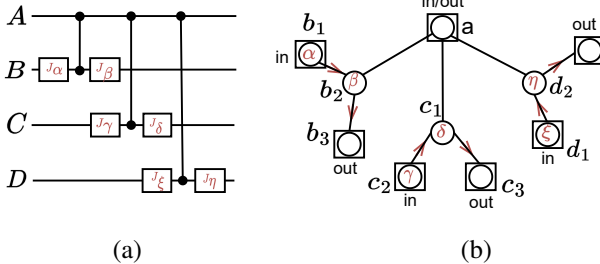


Fig. 2: Translation from a circuit (a) to its graph state (b), with the measurement bases labeled on the qubits in (b). The logical quit  $A$  corresponds to physical qubit  $a$  and  $B, C, D$  correspond to  $\{b_1, b_2, b_3\}, \{c_1, c_2, c_3\}$  and  $\{d_1, d_2, d_3\}$ , respectively. Qubits in (b) with ‘in’, ‘out’ or ‘in/out’ are input or output qubits. Arrows such as  $b_1 \rightarrow b_2$  indicate that the measurements of some qubits depend on the measurement outcomes of other qubits (e.g.,  $b_2$  depends on  $b_1$ ).

horizontal and vertical polarization of one photon), referred to as ‘polarization qubits’. Those two representations are mathematically equivalent and can be physically switched to each other using polarizing beam splitters [20]. Photonic quantum computing does not require an extremely low temperature compared with other quantum hardware technologies [2], [14], [17], [21], and is potentially highly scalable with the ability of constantly generating a large number of photons.

**Generating Cluster State** Large-scale one-way quantum computing requires a large cluster state to be prepared as a resource. There are two approaches to entangle photonic qubits and create cluster state upon them. One approach is to directly create entangled photons through nonlinear optical devices which induce interactions between photons and effectively lead to a deterministic cluster state generation. However, such nonlinear systems are difficult to scale [15], [20]. The second approach is to use linear optical devices and photon detectors to realize a special operation, namely fusion, which can merge two cluster states to construct a larger cluster state. This approach is readily CMOS compatible and easy to scale; nevertheless, it is at the cost of consuming two qubits in the two cluster states to be merged and is not deterministic. Significantly overhead is required if we need to construct a large cluster state with a high probability. Thus, recent efforts [4], [15] are to take advantages of both methods and reduce their shortcomings by combining them in the following way: A bunch of small entangled states can be generated deterministically using the first approach and then can be fused to construct a large cluster state.

**Fusion** The fusion operation [4], [10], [20] is a native gate on photonic device that can merge two cluster states through two joint measurement operations on two qubits from the two cluster states. For example, a joint measurement in the basis of  $XX, ZZ$  projects a state to the Bell basis, which creates entanglement between the qubits. The joint measurement we use in this paper is in  $XZ, ZX$  basis, which entangles two cluster states into a larger one at the cost of losing two photons.

In Figure 3, we use fusion operation to merge two two-qubit cluster states  $AC$  and  $BD$ . After the two joint measurements on qubits  $C$  and  $D$  are implemented, the two measured qubits are destroyed and the rest qubits  $A$  and  $B$  are now merged to one cluster state, which is a new two-qubit cluster state. In general, when we merge two cluster states with  $m$  and  $n$  qubits, the final cluster state after fusion will have  $m + n - 2$  qubits. Since fusion operations themselves are very costly [4], [10] and have the overhead of losing two qubits per fusion, one of the goals in our compiler is to minimize the number of fusion operations.

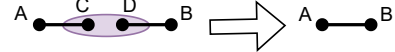


Fig. 3: A fusion between cluster states  $AC$  and  $BD$ . After the fusion (a  $XZ, ZX$  measurement on  $C, D$ ), qubit  $C, D$  vanish and qubit  $A, B$  form a new cluster state.

### III. PROBLEM FORMULATION

In this section, we first formulate the hardware abstraction of a linear photonic quantum computer and its compilation challenges. Then we provide an overview of our proposed framework.

#### A. Hardware Abstraction

We formulate a formal hardware model abstraction, namely the *flattened temporal-spatial hierarchy coupling graph* for a photonics based quantum computer, as shown in Fig. 4. This abstraction follows the hardware architecture from PsiQuantum [4], a leading industry in the area of photonic quantum computing. There are three levels of coupling in this graph and they are introduced as follows.

**Coupling in the resource state** The first level of coupling comes from qubits in the same *resource state*, i.e. the small cluster state generated by a resource state generator (RSG). Each node in Fig. 4 represents a resource state, which contains a few entangled qubits. Without loss of generality, the rest of the paper uses three-qubit GHZ states as the basic resource states generated by RSGs. Each RSG can repeatedly generate a resource state at every clock cycle.

**Coupling within a clock cycle** The second level of coupling comes from the resource states generated within the same clock cycle, which together form a layer of qubits referred to as a *physical layer*. As shown in Fig. 4, the nodes in the physical layer at  $t_0$  (or  $t_1, t_2$ ) are connected into a 2D lattice structure. Such connections within a clock cycle represent the spatial connections supported directly by the hardware. That is, a resource state generated by an RSG can conduct a fusion with resource states generated at the same clock cycle by its neighboring RSGs.

**Coupling across time frames** The third level of coupling is that a resource state can make a fusion with another resource state generated in a different clock cycle by the same RSG with the help of delay lines, as shown by the red and grey vertical lines in Fig. 4(a) (connections of distance larger than one are omitted). Note that we should avoid using long-range temporal

connections because photons suffer more from the loss error as they stay longer in the delay lines. The 3D structure of the connectivity as shown in Fig. 4(a) can be transformed to a flattened temporal-spatial hierarchy coupling graph as shown in Fig. 4(b), with every other physical layer (e.g., the physical layer at  $t_1$ ) being flipped in the horizontal direction. To keep the figure clear, some temporal connections are omitted for the rows other than the first. Using this coupling graph, we can define an *extended physical layer* by combining multiple physical layers and ignoring temporal connections among them except for some of those on the boundaries. For example, in Figure 4, physical layers at  $t_0, t_1$  and  $t_2$  form an extended physical layer when preserving all the spatial connections and only the temporal connections in red.

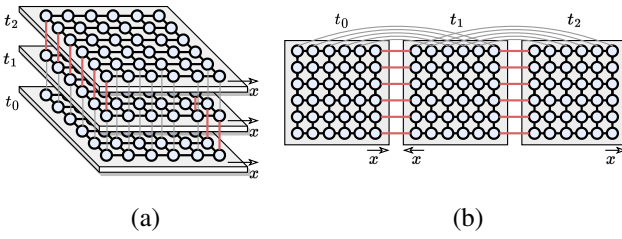


Fig. 4: 3D structure of hardware connectivity (a) and its flattened temporal-spatial hierarchy coupling graph (b). The physical layer  $t_1$  in (b) is flipped in the horizontal direction so that physical layers  $t_0, t_1$  and  $t_2$  form an extended physical layer by preserving all the spatial connections and only the temporal connections in red. To keep the figure clear, temporal connections of distance larger than 1 are omitted, some temporal connections of distance 1 are omitted in (b) as well except for the first row.

Despite the similarity to the quantum hardware coupling graph [23] prevailing used for today's superconducting and ion trap hardware architectures, we emphasize on their differences and our high-level insights behind such an abstraction.

- 1) The 3D connectivity structure is flattened into a series of 2D layers coming out constantly in the time axis, with each layer consisting of the resource states generated at a specific clock cycle. Successive layers can be chosen to form extended physical layers by preserving spatial connections within the layers and some of the temporal connection across the layer on the boundaries (red lines in Fig. 4). Within an extended physical layer, the time dimension is treated the same as a spatial dimension to enable the accommodation of larger size programs. This greatly simplifies the follow-up compilation optimization algorithm designs since the properties of planar graphs can be leveraged.
- 2) We remark that different levels of coupling are not independent of each other, and actually their interplay could create some additional constraints. For example, suppose the resource states generated by RSGs are 3-qubit GHZ states, then although the fusion device allows a RSG to maximally connect to 4 spatial neighbors (up,

down, left, right) and previous or future resource states generated by the same RSG within the range of delay lines, only up to 3 of them can be activated.

### B. Overview of Our Planar-Centric Compiler

Upon the abstracted linear photonic quantum hardware model above, we propose an end-to-end, planar-centric compilation framework that supports the mapping of any MBQC program to its execution pattern on our hardware model. By identifying the compilation challenges in this compilation flow, our framework consists of three major optimization modules, *Fusion Graph Generation* (Section IV), *2D-Lattice Mapping and Routing* (Section V), and *Graph Partition and Scheduling* (Section VI). We also remark that the planar graph theory [12], [18] plays an important role in our compiler design, and this is why we name it planar-centric compilation framework.

#### a) Objectives

As the first end-to-end compiler for MBQC, it is important to figure out a set of meaningful optimization goals. Our investigation on photonic one-way computing and realistic photonic quantum device development suggests the following two key optimization objectives.

- 1) **Minimizing the physical depth.** The physical depth is defined as the number of physical layers consumed in the computation, which represents the time of executing the compiled program.
- 2) **Reducing the number of fusions.** Fusions are often the most low-fidelity and costly operations incurred in such an MBQC photonic quantum computer.

#### b) Compiler Modules

In the rest of this section, we use a motivating example (shown in Figure 5) to give some high-level ideas about the key challenges being addressed by these three modules and the highlights of our technical contributions. We have attempted to maximize simplicity and ease of understanding, while possibly sacrificing some rigor. We often omit the dependency arrows and explicit measurement bases when they are not important for our optimization techniques, and they can always be derived from the graph state [9].

**Module 1: Fusion Graph Generation** This module focuses on strategies of synthesizing a graph state representing any input quantum circuit from resource states, as shown in Figure 5 (b) and (c), which can be further abstracted to *fusion graphs* that indicate necessary fusions at the granularity of resource states (e.g. Fig 8(c), 9(d)). It mainly tackles the constraints from the *limited inter-connections among individual photonic qubits in resource states*. This is important as a qubit conducting many two-qubit gates with other qubits (e.g. node G in Figure 5(a)) would naturally result in a high-degree qubit node in the graph state (e.g., node G in Figure 5(b)) and this could prevent us from executing the program on real hardware where only limited connections among qubits are provided. Our key insight is that those high-degree qubit nodes can be synthesized by a proper strategy of fusions between low-degree qubits in resource states (e.g., from node G in Figure 5(b) to the area around G in the central part of

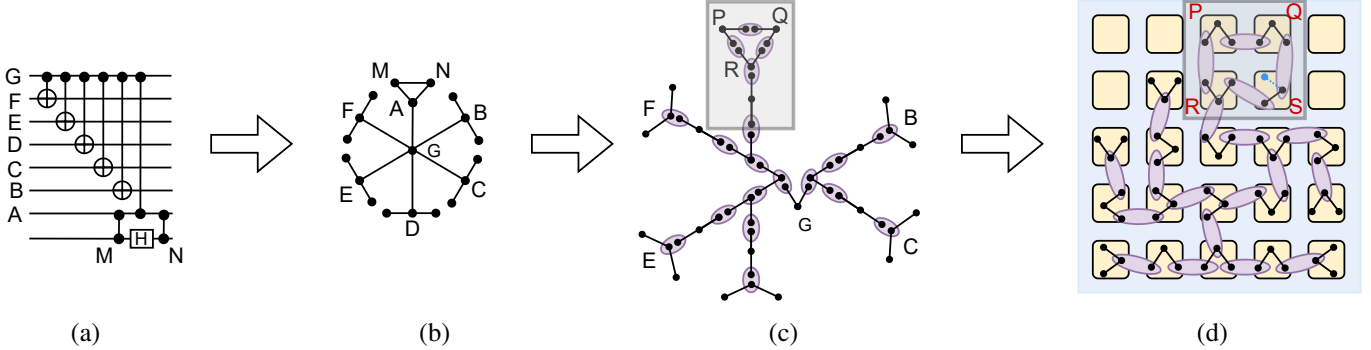


Fig. 5: Example of the compilation flow: (a) input circuit program; (b) graph state; (c) fusion graph generation; (d) 2D-lattice mapping and routing.

Figure 5(c)). By matching with some basic fusion patterns, arbitrary high-degree input graph states (Figure 5 (b)) can be synthesized to accommodate input adaptivity. Section IV gives detailed schemes for the generation of fusion graphs representing those synthesis strategies.

**Module 2: 2D-Lattice Mapping and Routing** In the next module we transform a fusion graph into a final embedding compatible with the topology of the hardware connectivity, in particular *the orthogonality of 2D lattice for potential fusion operations*. Example is shown in Fig. 5(c) and (d). In Fig. 5(c), the triangle consisting of resource states  $P$ ,  $Q$  and  $R$  (circled part in Fig. 5(c)) cannot be mapped to an orthogonal grid directly because  $R$  can not be adjacent to both  $P$  and  $Q$  if  $P$  and  $Q$  are mapped to adjacent RSG locations. Such incompatibility exist widely in a general fusion graph, which prevents a direct mapping from the fusion graph to the underlying hardware topology. Our insight is that such an issue can be resolved by extending some of the edges and winding them along the 2D lattice of individual or extended physical layers, which form paths of consecutive fusions. We refer to this procedure as routing. For example, in Fig. 5(d),  $P$ ,  $Q$  and  $R$  can conduct fusions with each other with an auxiliary resource state  $S$ . In  $S$ , two qubits participate in the routing path  $RSQ$ , with the other qubit (in blue) removed by a  $Z$ -measurement. By watching the available adjacent positions of each node on the lattice and penalizing long paths in a heuristic search, we can minimize the overhead induced by the extra fusions. Section V gives detailed searching schemes to map the edges onto orthogonal paths while minimizing the routing overhead.

**Module 3: Graph Partition and Scheduling** The third module addresses the conflict between *the large size of quantum programs and the small size of available resources* in each clock cycle limited by the generation speed and lifetime of resource states. The graphs for real-world quantum programs are too huge (in terms of their number of nodes and edges) to be mapped onto one or a few physical layers. In order to accommodate such large quantum programs on the hardware, careful partition and scheduling schemes are thus in demand for decomposing large input programs into smaller components which can then be synthesized and mapped onto the hardware by the two modules above. Our

insight is that both the program dependency and the graph topology should be taken into account to enable a more global optimization within the range of available resources. By balancing the leverage of global structure of the graph and the requirement for long-range temporal connections arising from the dependency relation, we can maximize the parallelism between operations while benefiting the efficiency of resource utilization. Section VI gives detailed schemes of partition and scheduling.

**All Modules: Non-Planar Graph Prohibition** The last challenge we identify is *non-planar graph prohibition*, which plays an important role in all three modules. By non-planar graph prohibition, we mean that the graph embedded into each physical layer should be a planar graph [12], i.e., a graph that can be drawn on a plane in a way that no edges cross each other. On one hand, this is because the small size of resource states and the limited physical connections among them prevent the routing paths on the lattice from crossing each other. On the other hand, we find the design philosophy motivated by this requirement powerful in suppressing the optimization space and thus leading to a more efficient heuristic search. The complexity of graph non-planarity can either arise directly from the input graphs (Figure. 6(b)) or indirectly from our optimization steps if not carefully designed (Fig. 9(e)). Our insight is that such a challenge can be tackled by (1) eliminating the non-planarity by decomposing each non-planar component to a set of planar graphs (Fig. 6 (c)), (2) enforcing our key modules to maintain such a planar property as an optimization. Details are incorporated in each section of the key modules, with the elimination included in Section VI and the enforcement included in Section IV, V.

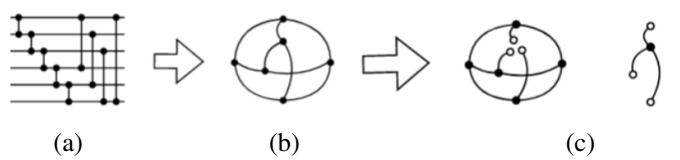


Fig. 6: A non-planar graph state (b) translated from a circuit (a), with the measurement basis omitted. The non-planar graph (b) can be broken into two planar sub-graphs in (c).

#### IV. FUSION GRAPH GENERATION

We start introducing our framework from a planar graph component that has been partitioned and scheduled from the input program. The key challenge at this step is to synthesize the high-degree nodes in the planar graphs from low-degree nodes that are directly supported by the hardware.

##### A. Basic Patterns

We start by defining a set of basic patterns, which will lay a foundation of supporting arbitrary graph states via small resource states. As shown in Fig. 7, the degree of a node  $V$  in a sub-graph can be incremented by applying a fusion between  $V$  and the root node of a resource state (Fig. 7(a)); the length of an edge from  $V$  can be extended by applying a fusion between  $V$  and a leaf node of a resource states (Fig. 7(b)). Hence an arbitrary graph can be synthesized by alternating those two basic patterns dynamically. Moreover, two synthesized graphs can be connected by applying a fusion between two leaf nodes of them (Fig. 7(c)). This plays the key role of connecting the sub-graphs scheduled in different rounds.

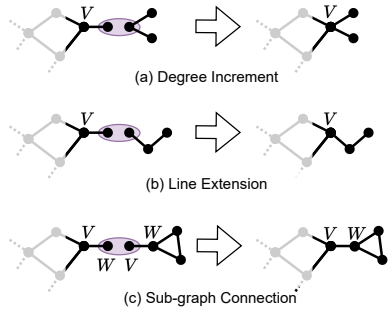


Fig. 7: (a) Increment the degree of a node. (b) Extend the length of a line. (c) Connecting two sub-graphs into a graph.

##### B. Graph synthesis

High degree nodes are prevalent in graph states of MBQC. For example, a logical qubit ( $G$  in Fig. 5(a)) involved in multiple CNOT gates in a circuit can result in a high degree node ( $G$  in Fig. 5(b)) in the corresponding graph state. Our framework supports such high degree nodes on small resource states via the basic pattern of degree increment (Fig. 7(a)). As shown in Fig. 8(a)(b), we can synthesize a high degree node by repeatedly fusing a lower degree node with the root node of a resource state until enough degree is obtained. In this way, a node of degree  $n$  can be synthesized from  $n - 1$  resource states.

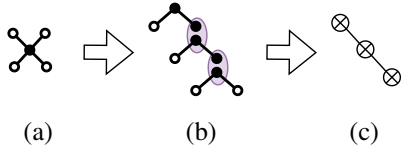


Fig. 8: Synthesize a high degree node in (a) by a basic fusion pattern in (b). Represent the fusion pattern by a fusion graph in (c), with each node representing a resource state, each edge representing a fusion operation

To synthesize a graph, we can first synthesize the high degree nodes in the above way and synthesize the low degree lines by the basic pattern of line extension (Fig. 7(b)). Then, the high degree nodes and lines can be connected via the basic pattern of sub-graph connection (Fig. 7(c)). We demonstrate it with an example of synthesizing a graph in Fig. 9(a). In Fig. 9(b), we break down the graph into high degree nodes  $A, B, C, D, O$  and lines  $PQ, RS$ . Each node high degree node or each line is connected with some nodes in hollowed dots, which represent its neighbors in Fig. 9(a). Those nodes are referred to as *virtual nodes*. Note that multiple virtual nodes are allowed to represent the same node, such as  $A, B, C, D, O$ . In Fig. 9(c), we pair up the virtual nodes according to the original graph Fig. 9(a) and synthesize the graph by applying the basic pattern of sub-graph connection (Fig. 7(c)) on the paired virtual nodes.

##### C. Optimized Fusion Graph

The fusion relations between small resource states in a synthesis pattern can be abstracted to a *fusion graph* by considering each resource state as a whole. For example, the synthesis pattern of a high degree node in Fig. 8(b) can be represented by a fusion graph in Fig. 8(c), with each node ‘ $\otimes$ ’ representing a resource state, and each edge representing a fusion between certain qubits of the resource states. With the breakdown of a graph state in Fig. 9(b), the fusion graph of the original graph Fig. 9(a) can be generated by substituting the high degree nodes to their corresponding fusion graphs (‘ $\otimes$ ’s in the same grey circle) as shown in Fig. 9(c).

Yet, not every fusion graph is equally good. We hope that the fusion graph generation does not break the planarity of the original graph due to a hardware constraint that will be introduced in Section V-A. Namely, the generated fusion graph of a planar graph should still be a planar graph, with a planar graph meaning that the graph can be drawn on a plane with edges not crossing each other. This can be achieved by first finding a planar embedding of the original graph, i.e. a way of drawing it on the plane with no crossing edges, and then replacing each high degree node with their linear fusion graphs while keeping the clockwise (counter-clockwise) orders among the neighbors of the high degree node.

For example, in the planar graph shown in Fig. 9(a), the 4-degree node  $O$  has neighbors  $B, A, C, D$  in a counter clockwise order, so we replace  $O$  with a fusion graph component of 3 nodes (the grey circle in the center of Fig. 9(e)), and join the nodes with  $B, A, C, D$  in a counter clockwise order (Fig. 9(d)). Note that the last node joins with both  $D$  and  $C$ . For the 3-degree node  $A$  (similarly for  $B, C, D$ ) with counter clockwise neighbors  $B, C, O$ , we replace it with a component of 2 nodes, and join the nodes with  $B, C, O$  in an counter clockwise order (Fig. 9(c)). As a comparison, Fig. 9(d) shows a fusion graph that breaks the planarity if not keeping the clockwise (counter-clockwise) orders.

#### V. 2D-LATTICE MAPPING AND ROUTING

The next step is to map each resource state in the fusion graph to a RSG location of a (extended) physical layer.

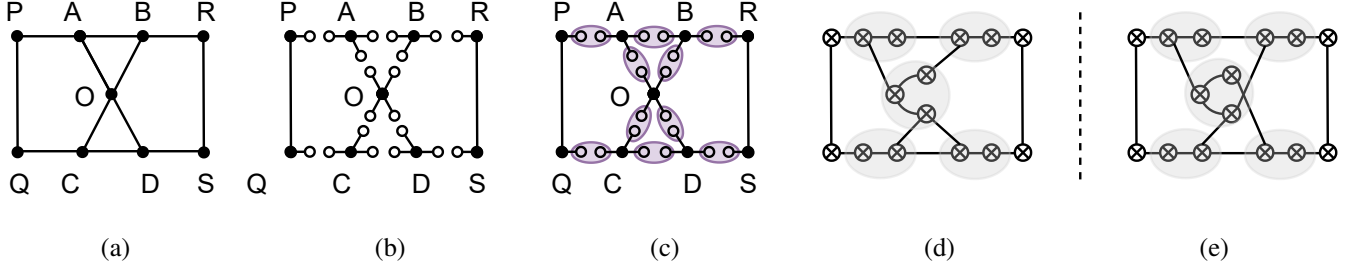


Fig. 9: A graph state (a) can be synthesized by first synthesizing high degree nodes with the basic pattern of degree increment and synthesizing lines with the basic pattern of line extension (obtaining (b)), then connecting them with the basic pattern of sub-graph connection as in (c). An optimized fusion graph of a planar graph (a) should still be planar, e.g. (d), while a random fusion graph may break the planarity, e.g. (e).

The main challenge is to fit the irregular structure of fusion graphs into the orthogonal structure of the spatial and temporal connectivity on the hardware.

#### A. Routing

*Routing* plays an important role in finding a 2D lattice mapping as it resolves the conflicts between the geometry of fusion graphs and the 2D lattice connections between the RSGs. In particular, it allows fusions between non-neighboring resources states by finding a path between them on the 2D lattice. For example, a triangular fusion graph as shown in the shaded area of Fig. 5(c) does not have a direct mapping onto the grid because when  $P, Q$  are mapped adjacently on the grid,  $R$  can be adjacent to at most one of them. However as shown in the shaded area of Fig. 5(d), when mapping  $R$  adjacent to  $P$ ,  $R$  can reach  $Q$  by routing via a path of consecutive fusions through  $S$  at the cost of consuming an extra resource state. In resource state  $S$ , two qubits participate in the fusions along the path, while the blue qubit is removed by a Z-measurement.

Specifically, routing resolves two types of conflicts in finding a 2D-lattice mapping. The first type occurs when mapping a new node onto the 2D-lattice if the neighboring locations of existing nodes cannot provide enough degrees, shown as the pink paths in Fig. 10(a). For example, in Fig. 10(a), if we want to map a node that connects to a mapped node  $B$  and two not-yet-mapped nodes  $E, F$ , then we should map it to location  $B'$  via a routing path through  $R_2$ . Because if we map it directly to  $R_2$ , i.e. the adjacent location of  $B$ , then there would not be enough adjacent locations to accommodate both  $E$  and  $F$  since there is only one location left around  $R_2$ . The second type of conflicts occurs when mapping an edge between two nodes already mapped to the 2D-lattice, shown as the pink paths in Fig. 10(b). Such cases arise from the cyclic structure of a graph. For example, to form a cycle as shown in the shaded area of Fig. 10(b), we need to connect the nodes by finding a shortest routing path  $A, B, C$ .

A hardware constraint for routing is that each resource state can be used by only one path due to its limited size, because each routing path consumes two qubits of every resource state along the path. This means that all routing paths should not cross each other in a 2D-lattice mapping. Namely, the fusion graph mapped to the 2D-lattice should be a planar graph.

#### B. Planar Mapping

We are now ready to introduce the algorithm that finds a mapping from a scheduled planar fusion graph to the 2D-lattice. We propose a heuristic search algorithm with a goal of finding a compact layout on the 2D-lattice.

We map the edges in a cycle-prioritized breadth-first order. That is, we map all the edges involved in cycles in a breadth-first order, along the way adding tree edges of each node once its cycle edges are all traversed. The insight behind it is that only the *planar orders* (i.e. clockwise or counter-clockwise orders) between cycle edges matter for a planar embedding, while the permutation among tree edges does not break the planarity. Every time when a new edge is mapped, a heuristic cost function  $H$  is used to rate the candidate layout. Then the layout with the lowest cost is selected and used to update the current layout. We design the heuristic cost function as

$$H = -\alpha \cdot \# \text{mapped\_edges} + \beta \cdot \text{routing\_length} + B$$

where  $\# \text{mapped\_edges}$  is the number of edges mapped onto the lattice and  $\text{routing\_length}$  is the total number of extra resource states consumed by all the routing paths, with  $\alpha, \beta$  being two hyper parameters. These two terms ranks the compactness of a candidate layout by rewarding the accommodation of more edges and penalizing the use of long routing paths.  $B$  is a look-ahead cost function that penalizes the congestion among nodes by comparing the number of remaining unmapped neighbors of each node and the number of its available adjacent locations that may accommodate those neighbors in a correct planar order.

There are two key optimizations for the heuristic search: planarity awareness and physical layer extension. First, the mapping of individual edges follows a planar embedding of the fusion graph found before the heuristic search so that it prevents routing paths from crossing each other and naturally increases the number of edges that can be accommodated by a physical layer. Second, the searching area can be adjusted dynamically by allowing an *extended physical layer* consisting of multiple physical layers. As shown in Fig. 4, a 3-layer extended physical layer can be obtained by ignoring the temporal connections among layer  $t_0, t_1, t_2$  except those between the resource states on the  $m$ -th column of layer  $t_0$  and layer  $t_1$ , and those between the resource states on the 0-th column

of layer  $t_1$  and layer  $t_2$ . This extension enables a more global optimization by allowing the mapping of a larger planar graph without being interrupted by the narrow boundaries.

### C. Non-Planar Shuffling

The overall philosophy of mapping is that each planar sub-graph of a fusion graph are mapped to a separate (extended) physical layer, and the connections between those planar components are addressed by a re-arrangement of the connecting nodes via routing paths on intermediate layers in between, called *shuffling*. For example, the two planar sub-graphs in Fig. 6(c) of the non-planar graph in Fig. 6(b) can be connected by joining their virtual nodes in pair.

To implement shuffling between the layouts of two planar sub-graphs, we first pair up their connecting nodes according to the original fusion graph, and sort the node pairs by their distances. Then we allocate one (or more) extra physical layers between the (extended) physical layers of those two layouts and find a shortest routing path between each pair of nodes in an ascending order of their distances.

## VI. GRAPH PARTITION AND SCHEDULING

In this section, we complete the entire flow by introducing how our framework partitions and schedules a general graph state. The challenges of partitioning and scheduling arise from the dependency relation in the measurements of the graph state and the non-planarity in the geometry of the graph.

### A. Program Dependency

Non-Clifford gates of a circuit prevent the corresponding MBQC measurement pattern from parallelism by inducing dependency among the measurement bases of qubits, represented by arrows in the graph state as in Fig. 2(b). Specifically, the measurement angles of the affected bases are adjusted from  $\alpha$  to  $(-1)^s\alpha + t\pi$  according to previous measurement outcomes, with the outcomes that affect  $s$  called  $X$ -dependency and those affecting  $t$  called  $Z$ -dependency [9]. With the fact that changing the angle from  $\alpha$  to  $\alpha + \pi$  only changes  $|\pm\alpha\rangle$  to  $|\mp\alpha\rangle$ , i.e., the  $Z$ -dependency is equivalent to a re-interpretation of the measurement outcome of the affected qubit, we define the executability as follows.

**Lemma 1.** *A measurement on a qubit in the graph state is executable if all its  $X$ -dependent qubits are measured and all the  $Z$ -dependent qubits of all its  $X$ -dependent qubits are measured.*

The qubits of a graph state can be partitioned to multiple *dependency layers* by the order of the time they become executable. To prevent qubits from waiting in delay lines for too long, a principle of scheduling is that the qubits in higher dependency layers should be scheduled later than those in lower dependency layers.

### B. Graph Non-Planarity

Another obstacle of parallelism is the fact that the sub-graphs scheduled onto each physical layer have to be planar due to the hardware constraint introduced in Section V-A. For example, a graph state as shown in Fig. 6(b) cannot be scheduled onto a single physical layer despite its small size. At least two

physical layers are needed by decomposing the graph into two planar graphs as shown in Fig. 6(c), with hollowed dots being the virtual nodes introduced in Section IV-B. To maximize the parallelism, a second principle for scheduling is that the sub-graph  $G_i$  of  $G$  scheduled onto each (extended) physical layer should be close to a maximal planar sub-graph, meaning that the addition of any edge  $e \in G - G_i$  breaks the planarity of  $G_i$ .

A frequent situation is that the sub-graphs in certain successive dependency layers are all planar. In this case we define the maximal planar sub-graph in a coarser grain in a sense that we combine those successive dependency layers until the addition of the next dependency layer breaks the planarity of the combined sub-graphs. Such a combined planar sub-graph can be scheduled onto an extended physical layer, as long as its size is within the range of physical layers limited by the length of delay lines.

### C. Algorithm for Partition and Scheduling

We propose a *planarize-and-merge* algorithm to address the program dependency and graph non-planarity. First, we partition the qubits of a given graph state into dependency layers  $\{L_1, L_2, \dots\}$  according to the order of their executability. Then for each non-planar layer  $L_i$ , we decompose it to multiple planar sub-graph  $L_i \rightarrow \{l_{i1}, l_{i2}, \dots\}$  by finding maximal planar sub-graphs each a time. After that, we combine the planarized sub-graphs into coarse grained maximal planar sub-graphs  $\{R_1, R_2, \dots\}$  and schedule one sub-graph at each round. Nodes in different rounds of sub-graphs are connected by virtual nodes using delay lines, as exemplified in Fig. 6(c) and Fig. 9(b). The details are shown as pseudo codes in Algorithm 1.

---

#### Algorithm 1: Planarize and Merge

---

```

Input: A graph state  $G$ 
Output: A list of sub-graphs  $R = []$ 
1  $planar\_graph\_list = [], r = [], R = [];$ 
2 while there are nodes in  $G$  not visited do
3    $L \leftarrow$  sub-graph of  $G$  consisting all executable nodes;
4   while there are nodes in  $L$  not visited do
5      $l \leftarrow$  maximal planar graph of  $L$ ;
6      $planar\_graph\_list.append(l);$ 
7   end
8 end
9 for each  $l$  in  $planar\_graph\_list$  do
10  if  $r \cup l$  is planar then
11     $r \leftarrow r \cup l$ 
12  else
13    Add virtual nodes to  $r$  according to  $G$ ;
14     $R.append(r);$ 
15     $r \leftarrow [];$ 
16 end

```

---

## VII. EVALUATION

### A. Experiment Setup

**Platform** We perform all experiments on a Manjaro Linux laptop with a  $4 \times$  Intel Core i7-7500U CPU and 8GB RAM. Other software includes Python 3.10.2 and Qiskit 0.18.3 [1].

**Baseline** We implement the baseline by simulating quantum circuits in the one-way model using the ‘mapping onto

TABLE I: Benchmark programs.

Name	# qubit	# gate	cluster area	physical area
Quantum Fourier Transform (QFT)	9	320	5x5	12x12
	16	1000	7x7	16x16
	25	2400	9x9	21x21
Quantum Approximate Optimization Alg (QAOA)	9	130	5x5	12x12
	16	400	7x7	16x16
	25	700	9x9	21x21
Bernstein Vazirani (BV)	100	300	19x19	43x43
	196	600	27x27	61x61
	324	1000	35x35	79x79

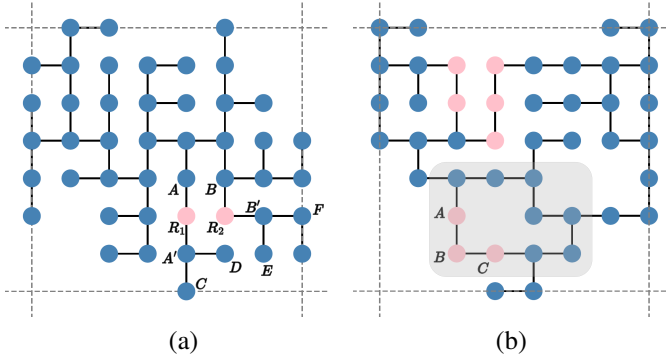


Fig. 10: (a) Mapping of fusion graph for 8-qubit BV with secret string '11111111'. (b) Mapping of fusion graph for 3-qubit QFT. Blue dots correspond to nodes '⊗' existing in the fusion graph, pink dots represents auxiliary resource states used for routing.

regular lattice first' approach as introduced in Section II-A1. There are two steps in the simulation. The first step is synthesizing a 3D cluster state with fusions from small resource states generated by the RSGs. For this step we use a lower bound by calculating the minimum number of resource states required to synthesize the large cluster state. The second step is simulating the state-of-the-art compiler [23] on the cluster state, with gates implemented with the measurement patterns introduced in Section II-A1.

**Benchmark programs** We select Quantum Fourier transform (QFT), quantum approximate optimization algorithm (QAOA) and Bernstein-Vazirani (BV) algorithm, the most typical application driven programs targeting at solving real-world problems as our benchmarks. For QAOA, we choose the graph maxcut problem on randomly generated graphs. For BV, we select the secret strings randomly. In Table I, we list the number of qubits and gates for each benchmark. We also list the minimum area of each layer of the cluster state required by the baseline as 'cluster area' and the minimum area of each physical layer required by the baseline as 'physical area'. We use the same physical area in the evaluation of our framework in order to compare with the baseline. The number of qubits we select are of the form  $n^2$  because that is the maximum number of logical qubits that can be accommodated by the area (qubit number between  $(n-1)^2 + 1$  and  $n^2$  all require the same area).

**Metric** As discussed in Section III-B, the first metric we consider is the physical depth, i.e., the number of physical

layers that are consumed by the compiled program. To make it comparable with the baseline, we assume that the number of RSGs on the hardware is the same as that is required by the implementing baseline. The second metric is the number of fusion operations executed by the compiled program, which is denoted as '# fusion'. A better compiler should compile a quantum program into a smaller depth which indicates a shorter execution time, and a smaller '# fusion' which indicates less consumption of resources and being less error-prone. For comparison, we define an improvement factor of physical depth as the ratio of the depth in the baseline and the depth in our framework, and an improvement factor of '#fusion' as the ratio of the number of fusions consumed in the baseline and the that consumed by our framework.

### B. Experiment Result

As shown in Table II, our framework achieves significant reduction in both physical depth and '# fusion' compared to the baseline. In specific, our framework reduces the physical depth on by a factor of 51.2 on average (geomean), up to 642.9. our framework also reduces the number of fusions by a factor of 420.9 on average (geomean), up to 20680.8.

Among the benchmarks, our framework has the most significant improvement for BV. The reasons are two folds. First, the graph state representation of BV in the one-way model contains no cycles and is thus completely planar. This naturally fits the planar-centric design of our framework. Second, the graph representation of BV contains a very high-degree node, i.e., as high as half of the number of qubits on average. In the simulation approach adopted by the baseline, that requires a huge number of inserted SWAP gates and thus waste a lot of physical layers. However, in our framework, it can be suppressed to a few of physical layers by a heuristic planar search that fully utilizes the resource states in those physical layers.

In contrast, the graph representations of QFT and QAOA contain a lot of short-range and long-range cycles, which not only makes the heuristic search much harder than that of BV, but also breaks the planarity of the graph. However, our framework still achieves a reduction on the physical depth by a factor of 16.7, 17.3, and a reduction on the number of fusions by a factor of 66.1, 84.2 for QFT and QAOA, respectively.

### C. Optimization Analysis

**Increase resource utilization** The significant improvements by our framework come from the increased utilization of resource states on each physical layer. To demonstrate, Fig. 10 shows the mappings of fusion graphs generated by our framework. Fig. 10(a) is a 8-qubit BV program mapped onto a 8x8 RSG grid while Fig. 10(b) is a 3-qubit QFT program mapped onto a 8x8 RSG grid. These two programs are two typical cases of acyclic structure and cyclic structure. In the figure, each dot represents a resource state. Dots in blue corresponds to the nodes '⊗' existing in the fusion graph, and the pink dots represent the auxiliary resource states used for routing. our framework enables a dense mapping that increases the utilization of each physical layer, in contrast to the sparse

TABLE II: The results of our framework and its relative performance to the baseline.

Name-#qubits	Baseline Depth	our framework Depth	Improv. Factor	Baseline #Fusions	our framework #Fusions	Improv. Factor
QFT-9	462	29	15.9	66,528	1,158	57.4
QFT-16	1,392	82	17.0	356,352	4,821	73.9
QFT-25	3,678	214	17.2	1,621,998	18,143	89.4
QAOA-9	426	23	18.5	61,344	911	67.3
QAOA-16	1,050	60	17.5	268,800	2,979	90.2
QAOA-25	1,584	99	16.0	698,544	7,336	95.2
BV-100	1,290	4	322.5	2,385,210	437	5458.1
BV-196	2,142	5	428.4	7,970,382	801	9950.5
BV-324	4,500	7	642.9	28,084,500	1,358	20680.8

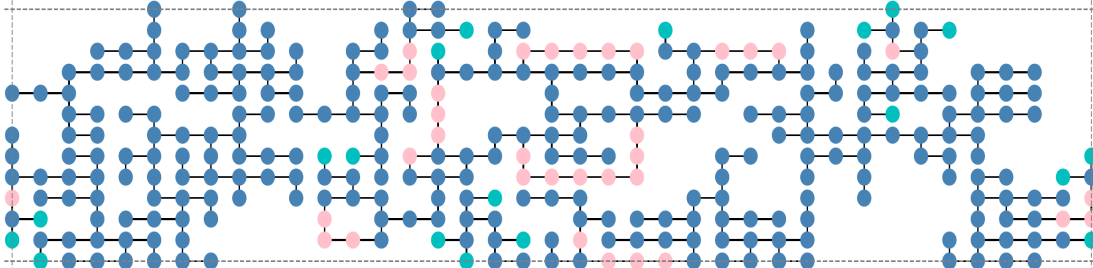


Fig. 11: Mapping of the fusion graph of a 16-qubit QFT program with a more global optimization by considering an extended physical layer consisting of 3 successive physical layers of size  $13 \times 13$ . Blue and green dots correspond to the nodes ‘ $\otimes$ ’ existing in the fusion graph, with the green ones being the incomplete nodes whose edges are not all mapped yet. Pink dots represent the auxiliary resource states used for routing.

mapping in the baseline caused by the rigid pattern of mapping and the large amount of preserved Z-measurement qubits.

**Flexible Physical Area** Besides the improvement in performance, our framework also enables a lower constraint and more flexibility to the varying size of physical layers. In comparison with the fixed sizes of physical layers required by the baseline approach caused by the fixed locations of logical qubits, our framework does not put a strict constraint on the size of physical layers. Our framework can compile the program onto a much smaller physical hardware than the baseline, with a trade-off of more physical layers. For example, Fig. 11 shows a slice of fusion graph mapping of a 16-qubit QFT program on three physical layers each with 169 resource states, which is much smaller than the physical layers of 256 resource states required by the baseline. Moreover, when the physical layers are larger than required by the baseline, the simulation approach has no way to utilize the extra resource, while our framework allows an optimization by spanning the mapping all over the physical layers.

**More Global Optimization** With the flattened temporal-spatial hierarchy coupling graph proposed in Section III-A (Fig. 4), our framework also enables a more global optimization in the mapping by searching through an extended physical layer composed by multiple physical layers. As a demonstration, Fig. 11 shows a slice of mapping generated by our framework for a 16-qubit QFT program. The whole rectangular  $13 \times 39$  plane is composed of 3 layers of  $13 \times 13$  resource state grid (much smaller than the  $16 \times 16$  physical layers required by the baseline). The first physical layer ranges from column 1 to column 13, the second ranges from column 14 to column 26, and the third from column 27 to column 39

respectively. In the figure, blue and green dots correspond to the nodes ‘ $\otimes$ ’ existing in the fusion graph, with the green ones representing the incomplete nodes, which means that some of edges connected to them have not been mapped onto the grid. Again, pink dots represent the auxiliary resource states used for routing.

As can be seen, the mapping onto extended physical layers enables an optimization by allowing long-range structures (e.g., long-range cycles crossing the boundaries of individual physical layers, i.e., column 13,14 and column 26,27) in the mapping, at a cost of sacrificing some inter-layer connections not on the boundaries. Moreover, this mapping strategy onto extended physical layers also reduces the searching space from a 3D grid to a large 2D grid, which significantly improves the compilation efficiency without much loss of performance.

## VIII. CONCLUSION

In this work, we give in-depth analysis and discussion of the unique challenges for photonic one-way computing at both programming and hardware levels. We build the first end-to-end compilation framework for optimizing the mapping of any quantum programs onto photonic devices supported by our hardware abstract model. With this being said, many of the optimization problems here are NP-hard problems, and thus we believe there are still large room for fully tapping the entire optimization space. As the first work in this direction, we hope our work could attract more efforts from the high-performance computer architecture and compiler community to explore the advantage of photonic quantum architectures and overcome the unique challenges.

## REFERENCES

- [1] M. S. ANIS, H. Abraham, AduOffei, R. Agarwal, G. Agliardi, M. Aharoni, I. Y. Akhalwaya, G. Aleksandrowicz, T. Alexander, M. Amy, S. Anagolum, E. Arbel, A. Asfaw, A. Athalye, A. Avkhadiev, C. Azaustre, P. Bhole, A. Banerjee, S. Banerjee, W. Bang, A. Bansal, P. Barkoutsos, A. Barnawal, G. Barron, G. S. Barron, L. Bello, Y. Ben-Haim, M. C. Bennett, D. Bevenius, D. Bhatnagar, A. Bhobe, P. Bianchini, L. S. Bishop, C. Blank, S. Bolos, S. Bopardikar, S. Bosch, S. Brandhofer, Brandon, S. Bravyi, N. Bronn, Bryce-Fuller, D. Bucher, A. Burov, F. Cabrera, P. Calpin, L. Capelluto, J. Carballo, G. Carrascal, A. Carriker, I. Carvalho, A. Chen, C.-F. Chen, E. Chen, J. C. Chen, R. Chen, F. Chevallier, K. Chinda, R. Cholaraian, J. M. Chow, S. Churchill, CisterMoke, C. Claus, C. Clauss, C. Clothier, R. Cocking, R. Cocuzzo, J. Connor, F. Correa, A. J. Cross, A. W. Cross, S. Cross, J. Cruz-Benito, C. Culver, A. D. Córcoles-Gonzales, N. D. S. Dague, T. E. Dandachi, A. N. Dangwal, J. Daniel, M. Daniels, M. Dartailh, A. R. Davila, F. Debouni, A. Dekusar, A. Deshmukh, M. Deshpande, D. Ding, J. Doi, E. M. Dow, E. Drechsler, E. Dumitrescu, K. Dumon, I. Duran, K. EL-Safty, E. Eastman, G. Eberle, A. Ebrahimi, P. Eendebak, D. Egger, ElePT, Emilio, A. Espiricueta, M. Everitt, D. Facoetti, Farida, P. M. Fernández, S. Ferracin, D. Ferrari, A. H. Ferrera, R. Fouilland, A. Frisch, A. Fuhrer, B. Fuller, M. GEORGE, J. Gacon, B. G. Gago, C. Gambella, J. M. Gambetta, A. Gammanpila, L. Garcia, T. Garg, S. Garion, J. R. Garrison, T. Gates, L. Gil, A. Gilliam, A. Giridharan, J. Gomez-Mosquera, Gonzalo, S. de la Puente González, J. Gorzinski, I. Gould, D. Greenberg, D. Grinko, W. Guan, D. Guijo, J. A. Gunnels, H. Gupta, N. Gupta, J. M. Günther, M. Haglund, I. Haide, I. Hamamura, O. C. Hamido, F. Harkins, K. Hartman, A. Hasan, V. Havlicek, J. Hellmers, L. Herok, S. Hillmich, H. Horii, C. Howington, S. Hu, W. Hu, J. Huang, R. Huisman, H. Imai, T. Imamichi, K. Ishizaki, Ishwor, R. Iten, T. Itoko, A. Ivrii, A. Javadi, A. Javadi-Abhari, W. Javed, Q. Jianhua, M. Jivrajani, K. Johns, S. Johnstun, Jonathan-Shoemaker, JosDenmark, JoshDumo, J. Judge, T. Kachmann, A. Kale, N. Kanazawa, J. Kane, Kang-Bae, A. Kapila, A. Karazeev, P. Kassebaum, J. Kelso, S. Kelso, V. Khanderao, S. King, Y. Kobayashi, Kovi11Day, A. Kovyrshin, R. Krishnakumar, V. Krishnan, K. Krsulich, P. Kumkar, G. Kus, R. LaRose, E. Lacal, R. Lambert, H. Landa, J. Lapeyre, J. Latone, S. Lawrence, C. Lee, G. Li, J. Lishman, D. Liu, P. Liu, A. K. M. L. Madden, Y. Maeng, S. Maheshkar, K. Majmudar, A. Malyshev, M. E. Mandouh, J. Manela, Manjula, J. Marecek, M. Marques, K. Marwaha, D. Maslov, P. Maszota, D. Mathews, A. Matsuo, F. Mazhandu, D. McClure, M. McElaney, C. McGarry, D. McKay, D. McPherson, S. Meesala, D. Meirom, C. Mendell, T. Metcalfe, M. Mevissen, A. Meyer, A. Mezzacapo, R. Midha, D. Miller, Z. Minev, A. Mitchell, N. Moll, A. Montanez, G. Monteiro, M. D. Mooring, R. Morales, N. Moran, D. Morcuende, S. Mostafa, M. Motta, R. Moyard, P. Murali, J. Müggenburg, T. NEMOZ, D. Nadlinger, K. Nakanishi, G. Nannicini, P. Nation, E. Navarro, Y. Naveh, S. W. Neagle, P. Neuweiler, A. Ngoueya, J. Nicander, Nick-Singstock, P. Niroula, H. Norlen, NuoWenLei, L. J. O’ Riordan, O. Ogunbayo, P. Ollitrault, T. Onodera, R. Otaolea, S. Oud, D. Padilha, H. Paik, S. Pal, Y. Pang, A. Panigrahi, V. R. Pascuzzi, S. Perriello, E. Peterson, A. Phan, K. Pilch, F. Piro, M. Pistoia, C. Piveteau, J. Plewa, P. Poreau, A. Pozas-Kerstjens, R. Pracht, M. Prokop, V. Prutyanov, S. Puri, D. Puzzuoli, J. Pérez, Quant02, Quintii, R. I. Rahman, A. Raja, R. Rajeev, I. Rajput, N. Ramagiri, A. Rao, R. Raymond, O. Reardon-Smith, R. M.-C. Redondo, M. Reuter, J. Rice, M. Riedemann, Rietesh, D. Risinger, M. L. Rocca, D. M. Rodríguez, RohithKarur, B. Rosand, M. Rossmannek, M. Ryu, T. SAPV, N. R. C. Sa, A. Saha, A. Ash-Saki, S. Sanand, M. Sandberg, H. Sandesara, R. Sapra, H. Sargsyan, A. Sarkar, N. Sathaye, B. Schmitt, C. Schnabel, Z. Schoenfeld, T. L. Scholten, E. Schoute, M. Schulterbrandt, J. Schwarm, J. Seaward, Sergi, I. F. Sertage, K. Setia, F. Shah, N. Shammah, R. Sharma, Y. Shi, J. Shoemaker, A. Silva, A. Simonetto, D. Singh, D. Singh, P. Singh, P. Singkanipa, Y. Siraichi, Siri, J. Sistos, I. Sitzikov, S. Sivarajah, M. B. Sletfjording, J. A. Smolin, M. Soeken, I. O. Sokolov, I. Sokolov, V. P. Soloviev, SooluThomas, Starfish, D. Steenken, M. Stypulkoski, A. Suau, S. Sun, K. J. Sung, M. Suwama, O. Slowik, H. Takahashi, T. Takawale, I. Tavernelli, C. Taylor, P. Taylor, S. Thomas, K. Tian, M. Tillet, M. Tod, M. Tomasic, C. Tornow, E. de la Torre, J. L. S. Toural, K. Trabing, M. Treinish, D. Trenev, TrishaPe, F. Truger, G. Tsilimkounakis, D. Tulsi, W. Turner, Y. Vaknin, C. R. Valcarce, F. Varchon, A. Vartak, A. C. Vazquez, P. Vijaywargiya, V. Villar, B. Vishnu, D. Vogt-Lee, C. Vuillot, J. Weaver, J. Weidenfeller, R. Wieczorek, J. A. Wildstrom, J. Wilson, E. Winston, WinterSoldier, J. J. Woehr, S. Woerner, R. Woo, C. J. Wood, R. Wood, S. Wood, J. Wootton, M. Wright, L. Xing, J. YU, B. Yang, U. Yang, D. Yerlin, R. Yonekura, D. Yonge-Mallo, R. Yoshida, R. Young, J. Yu, L. Yu, C. Zachow, L. Zdanski, H. Zhang, I. Zidaru, and C. Zoufal, “Qiskit: An open-source framework for quantum computing,” 2021.
- [2] T. Asselmeyer-Maluga, “3d topological quantum computing,” *International Journal of Quantum Information*, 2021.
- [3] S. Bartolucci, P. Birchall, H. Bombin, H. Cable, C. Dawson, M. Gimeno-Segovia, E. Johnston, K. Kieling, N. Nickerson, M. Pant, F. Pastawski, T. Rudolph, and C. Sparrow, “Fusion-based quantum computation,” *arXiv preprint arXiv:2101.09310*, 2021.
- [4] S. Bartolucci, P. Birchall, H. Bombin, H. Cable, C. Dawson, M. Gimeno-Segovia, E. Johnston, K. Kieling, N. Nickerson, M. Pant, F. Pastawski, T. Rudolph, and C. Sparrow, “Fusion-based quantum computation,” *arXiv preprint 2101.09310*, 2021.
- [5] S. Bartolucci, P. Birchall, D. Bonneau, H. Cable, M. Gimeno-Segovia, K. Kieling, N. Nickerson, T. Rudolph, and C. Sparrow, “Switch networks for photonic fusion-based quantum computing,” *arXiv preprint arXiv:2109.13760*, 2021.
- [6] S. Bogdanov, M. Y. Shalaginov, A. Boltasseva, and V. M. Shalaev, “Material platforms for integrated quantum photonics,” *Opt. Mater. Express*, vol. 7, no. 1, pp. 111–132, Jan 2017. [Online]. Available: <http://opg.optica.org/ome/abstract.cfm?URI=ome-7-1-111>
- [7] H. Bombin, I. H. Kim, D. Litinski, N. Nickerson, M. Pant, F. Pastawski, S. Roberts, and T. Rudolph, “Interleaving: Modular architectures for fault-tolerant photonic quantum computing,” *arXiv preprint arXiv:2103.08612*, 2021.
- [8] H. J. Briegel, D. E. Browne, W. Dür, R. Raussendorf, and M. Van den Nest, “Measurement-based quantum computation,” *Nature Physics*, vol. 5, no. 1, pp. 19–26, 2009.
- [9] A. Broadbent and E. Kashefi, “Parallelizing quantum circuits,” *Theoretical computer science*, vol. 410, no. 26, pp. 2489–2510, 2009.
- [10] D. E. Browne and T. Rudolph, “Resource-efficient linear optical quantum computation,” *Physical Review Letters*, vol. 95, no. 1, p. 010501, 2005.
- [11] C. D. Bruzewicz, J. Chiaverini, R. McConnell, and J. M. Sage, “Trapped-ion quantum computing: Progress and challenges,” *Applied Physics Reviews*, vol. 6, no. 2, p. 021314, 2019.
- [12] N. Chiba, T. Nishizeki, S. Abe, and T. Ozawa, “A linear algorithm for embedding planar graphs using pq-trees,” *Journal of computer and system sciences*, vol. 30, no. 1, pp. 54–76, 1985.
- [13] M. H. Devoret and R. J. Schoelkopf, “Superconducting circuits for quantum information: an outlook,” *Science*, vol. 339, no. 6124, pp. 1169–1174, 2013.
- [14] D. P. DiVincenzo and Ibm, “The physical implementation of quantum computation,” *Protein Science*, vol. 48, pp. 771–783, 2000.
- [15] M. Gimeno-Segovia, P. Shadbolt, D. E. Browne, and T. Rudolph, “From three-photon ghz states to universal ballistic quantum computation,” 2015.
- [16] L. K. Grover, “A fast quantum mechanical algorithm for database search,” in *Proceedings of the twenty-eighth annual ACM symposium on Theory of computing*, 1996, pp. 212–219.
- [17] J. Kelly, “A Preview of Bristlecone, Google’s New Quantum Processor,” <https://ai.googleblog.com/2018/03/a-preview-of-bristlecone-googles-new.html>, 2017.
- [18] K.-i. Kawarabayashi and B. Reed, “Computing crossing number in linear time,” in *Proceedings of the thirty-ninth annual ACM symposium on Theory of computing*, 2007, pp. 382–390.
- [19] P. Kok, W. J. Munro, K. Nemoto, T. C. Ralph, J. P. Dowling, and G. J. Milburn, “Linear optical quantum computing with photonic qubits,” *Reviews of modern physics*, vol. 79, no. 1, p. 135, 2007.
- [20] P. Kok, W. J. Munro, K. Nemoto, T. C. Ralph, J. P. Dowling, and G. J. Milburn, “Linear optical quantum computing with photonic qubits,” *Reviews of modern physics*, vol. 79, no. 1, p. 135, 2007.
- [21] P. Kok, W. J. Munro, K. Nemoto, T. C. Ralph, J. P. Dowling, and G. J. Milburn, “Linear optical quantum computing with photonic qubits,” *Reviews of Modern Physics*, vol. 79, pp. 135–174, 2007.
- [22] M. V. Larsen, X. Guo, C. R. Breum, J. S. Neergaard-Nielsen, and U. L. Andersen, “Deterministic multi-mode gates on a scalable photonic quantum computing platform,” *Nature Physics*, vol. 17, no. 9, pp. 1018–1023, 2021.
- [23] G. Li, Y. Ding, and Y. Xie, “Tackling the qubit mapping problem for nisq-era quantum devices,” in *Proceedings of the Twenty-Fourth*

- [24] L. S. Madsen, F. Laudenbach, M. F. Askarani, F. Rortais, T. Vincent, J. F. F. Bulmer, F. M. Miato, L. Neuhaus, L. G. Helt, M. J. Collins, A. E. Lita, T. Gerrits, S. W. Nam, V. D. Vaidya, M. Menotti, I. Dhand, Z. Vernon, N. Quesada, and J. Lavoie, “Quantum computational advantage with a programmable photonic processor,” *Nature*, vol. 606, no. 7912, pp. 75–81, Jun 2022. [Online]. Available: <https://doi.org/10.1038/s41586-022-04725-x>
- [25] M. A. Nielsen and I. Chuang, “Quantum computation and quantum information,” 2002.
- [26] J. L. O’Brien, A. Furusawa, and J. Vučković, “Photonic quantum technologies,” *Nature Photonics*, vol. 3, no. 12, pp. 687–695, 2009.
- [27] J. L. O’Brien, A. Furusawa, and J. Vučković, “Photonic quantum technologies,” *Nature Photonics*, vol. 3, no. 12, p. 687, 2009.
- [28] M. Pant, D. Towsley, D. Englund, and S. Guha, “Percolation thresholds for photonic quantum computing,” *Nature communications*, vol. 10, no. 1, pp. 1–11, 2019.
- [29] R. Raussendorf, “Measurement-based quantum computation with cluster states,” *International Journal of Quantum Information*, vol. 7, no. 06, pp. 1053–1203, 2009.
- [30] R. Raussendorf, D. E. Browne, and H. J. Briegel, “Measurement-based quantum computation on cluster states,” *Physical review A*, vol. 68, no. 2, p. 022312, 2003.
- [31] M. Saffman, “Quantum computing with atomic qubits and rydberg interactions: progress and challenges,” *Journal of Physics B: Atomic, Molecular and Optical Physics*, vol. 49, no. 20, p. 202001, 2016.
- [32] P. W. Shor, “Polynomial-time algorithms for prime factorization and discrete logarithms on a quantum computer,” *SIAM review*, vol. 41, no. 2, pp. 303–332, 1999.
- [33] S. Sivarajah, S. Dilkes, A. Cowtan, W. Simmons, A. Edgington, and R. Duncan, “tl ket>: a retargetable compiler for nisq devices,” *Quantum Science and Technology*, vol. 6, no. 1, p. 014003, 2020.
- [34] S. Takeda and A. Furusawa, “Toward large-scale fault-tolerant universal photonic quantum computing,” *APL Photonics*, vol. 4, no. 6, p. 060902, 2019.
- [35] M. Van den Nest, A. Miyake, W. Dür, and H. J. Briegel, “Universal resources for measurement-based quantum computation,” *Physical review letters*, vol. 97, no. 15, p. 150504, 2006.
- [36] J. Wang, F. Sciarrino, A. Laing, and M. G. Thompson, “Integrated photonic quantum technologies,” *Nature Photonics*, vol. 14, no. 5, pp. 273–284, 2020.
- [37] H.-S. Zhong, Y.-H. Deng, J. Qin, H. Wang, M.-C. Chen, L.-C. Peng, Y.-H. Luo, D. Wu, S.-Q. Gong, H. Su, Y. Hu, P. Hu, X.-Y. Yang, W.-J. Zhang, H. Li, Y. Li, X. Jiang, L. Gan, G. Yang, L. You, Z. Wang, L. Li, N.-L. Liu, J. J. Renema, C.-Y. Lu, and J.-W. Pan, “Phase-programmable gaussian boson sampling using stimulated squeezed light,” *Phys. Rev. Lett.*, vol. 127, p. 180502, Oct 2021. [Online]. Available: <https://link.aps.org/doi/10.1103/PhysRevLett.127.180502>
- [38] H.-S. Zhong, H. Wang, Y.-H. Deng, M.-C. Chen, L.-C. Peng, Y.-H. Luo, J. Qin, D. Wu, X. Ding, Y. Hu, P. Hu, X.-Y. Yang, W.-J. Zhang, H. Li, Y. Li, X. Jiang, L. Gan, G. Yang, L. You, Z. Wang, L. Li, N.-L. Liu, C.-Y. Lu, and J.-W. Pan, “Quantum computational advantage using photons,” *Science*, vol. 370, no. 6523, pp. 1460–1463, 2020.